AMERICAN SOCIETY FOR MICROBIOLOGY | Journal of Virology®

VACCINES AND ANTIVIRAL AGENTS

Small-Molecule Antiviral β-D-N^4-Hydroxycytidine Inhibits a Proofreading-Intact Coronavirus with a High Genetic Barrier to Resistance

Maria L. Agostini,[a] Andrea J. Pruijssers,[b] James D. Chappell,[b] Jennifer Gribble,[a] Xiaotao Lu,[b] Erica L. Andres,[b] Gregory R. Bluemling,[c] Mark A. Lockwood,[c] Timothy P. Sheahan,[d] Amy C. Sims,[d] Michael G. Natchus,[c] Manohar Saindane,[c] Alexander A. Kolykhalov,[c] George R. Painter,[c,e] Ralph S. Baric,[d] Mark R. Denison[a,b]

[a]Department of Pathology, Microbiology, and Immunology, Vanderbilt University School of Medicine, Nashville, Tennessee, USA
[b]Department of Pediatrics, Vanderbilt University School of Medicine, Nashville, Tennessee, USA
[c]Emory Institute for Drug Development, Emory University, Atlanta, Georgia, USA
[d]Department of Epidemiology, University of North Carolina at Chapel Hill, Chapel Hill, North Carolina, USA
[e]Department of Pharmacology and Chemical Biology, Emory University School of Medicine, Atlanta, Georgia, USA

ABSTRACT Coronaviruses (CoVs) have emerged from animal reservoirs to cause severe and lethal disease in humans, but there are currently no FDA-approved antivirals to treat the infections. One class of antiviral compounds, nucleoside analogues, mimics naturally occurring nucleosides to inhibit viral replication. While these compounds have been successful therapeutics for several viral infections, mutagenic nucleoside analogues, such as ribavirin and 5-fluorouracil, have been ineffective at inhibiting CoVs. This has been attributed to the proofreading activity of the viral 3′-5′ exoribonuclease (ExoN). β-D-N^4-Hydroxycytidine (NHC) (EIDD-1931; Emory Institute for Drug Development) has recently been reported to inhibit multiple viruses. Here, we demonstrate that NHC inhibits both murine hepatitis virus (MHV) (50% effective concentration [EC_{50}] = 0.17 μM) and Middle East respiratory syndrome CoV (MERS-CoV) (EC_{50} = 0.56 μM) with minimal cytotoxicity. NHC inhibited MHV lacking ExoN proofreading activity similarly to wild-type (WT) MHV, suggesting an ability to evade or overcome ExoN activity. NHC inhibited MHV only when added early during infection, decreased viral specific infectivity, and increased the number and proportion of G:A and C:U transition mutations present after a single infection. Low-level NHC resistance was difficult to achieve and was associated with multiple transition mutations across the genome in both MHV and MERS-CoV. These results point to a virus-mutagenic mechanism of NHC inhibition in CoVs and indicate a high genetic barrier to NHC resistance. Together, the data support further development of NHC for treatment of CoVs and suggest a novel mechanism of NHC interaction with the CoV replication complex that may shed light on critical aspects of replication.

IMPORTANCE The emergence of coronaviruses (CoVs) into human populations from animal reservoirs has demonstrated their epidemic capability, pandemic potential, and ability to cause severe disease. However, no antivirals have been approved to treat these infections. Here, we demonstrate the potent antiviral activity of a broad-spectrum ribonucleoside analogue, β-D-N^4-hydroxycytidine (NHC), against two divergent CoVs. Viral proofreading activity does not markedly impact sensitivity to NHC inhibition, suggesting a novel interaction between a nucleoside analogue inhibitor and the CoV replicase. Further, passage in the presence of NHC generates only low-level resistance, likely due to the accumulation of multiple potentially deleterious transition mutations. Together, these data support a mutagenic mechanism of inhibition by NHC and further support the development of NHC for treatment of CoV infections.

Citation Agostini ML, Pruijssers AJ, Chappell JD, Gribble J, Lu X, Andres EL, Bluemling GR, Lockwood MA, Sheahan TP, Sims AC, Natchus MG, Saindane M, Kolykhalov AA, Painter GR, Baric RS, Denison MR. 2019. Small-molecule antiviral β-D-N^4-hydroxycytidine inhibits a proofreading-intact coronavirus with a high genetic barrier to resistance. J Virol 93:e01348-19. https://doi.org/10.1128/JVI.01348-19.

Editor Tom Gallagher, Loyola University Chicago

Address correspondence to Mark R. Denison, mark.denison@vumc.org.

Received 14 August 2019
Accepted 24 September 2019
Accepted manuscript posted online 2 October 2019
Published 26 November 2019

KEYWORDS coronavirus, nucleoside analogue, RdRp, RNA-dependent RNA polymerase, SARS-CoV, MERS-CoV, pandemic, antiviral resistance

The emergence of severe acute respiratory syndrome (SARS) in 2002 and Middle East respiratory syndrome (MERS) in 2012 has underscored the ability of coronaviruses (CoVs) to cause lethal disease in humans (1, 2). MERS-CoV continues to infect humans in the Middle East, and four additional human CoVs (HCoVs), HCoV-229E, HCoV-NL63, HCoV-OC43, and HCoV-HKU1, continue to circulate globally and cause respiratory disease (3–6). The continued circulation in bat populations of SARS- and MERS- like CoVs that can replicate efficiently in primary human airway cells further demonstrates the potential for CoVs to emerge and cause severe disease in the future (7–10). While SARS-CoV and MERS-CoV outbreaks have been controlled, largely through public health measures (11–13), the potential for future outbreaks highlights the need for safe and effective therapeutics to combat CoV infections. There are currently no approved therapeutics or vaccines for any human CoV infection. Previous efforts to treat CoV infections with existing antivirals did not conclusively benefit clinical outcomes; thus, the current standard of care remains mostly supportive (14–16).

Several targets for direct-acting antivirals are being investigated to treat CoV infections (17–19). Because the viral replication machinery performs an essential role in genome replication, therapeutics approved to treat multiple different viral infections are aimed at this target (20). Many approved antivirals are classified as nucleoside analogues, compounds that mimic natural nucleosides to inhibit viral replication (21). Inhibition by nucleoside analogues can be accomplished through a variety of mechanisms. Common mechanisms of action include incorporation of the analogue by the viral polymerase to induce premature termination of strand synthesis and loss of essential genetic information through mutagenesis (22–25). A previous study reported that the nucleoside analogues ribavirin (RBV) and 5-fluorouracil (5-FU) did not potently inhibit CoVs, and this finding was attributed to the proofreading capabilities of the viral 3′-5′ exoribonuclease (ExoN) (26). Recent reports have demonstrated the inhibition of wild-type (WT) CoVs by nucleoside analogues such as galidesivir (BCX4430) and remdesivir (GS-5734) (27–29). While these compounds have shown efficacy against CoVs, administration of multiple compounds simultaneously may be required to effectively treat CoV infections and control the emergence of drug resistance, as has been demonstrated for other viral infections (30).

β-D-N^4-Hydroxycytidine (NHC) (EIDD-1931; Emory Institute for Drug Development), a cytidine analogue, has recently been shown to inhibit multiple viruses, including chikungunya virus, Venezuelan equine encephalitis virus (VEEV), respiratory syncytial virus (RSV), hepatitis C virus, norovirus, influenza A (IAV) and B viruses, and Ebola virus (31–36). Previous reports have demonstrated increased introduction of transition mutations in viral genomes after treatment, as well as a high genetic barrier to resistance (31, 36). Antiviral activity of NHC has also been reported against the human α-CoV HCoV-NL63, as well as the β-CoV SARS-CoV (43, 44). Neither the NHC mechanism of action nor NHC resistance has been described for any CoV to date.

In this study, we investigated NHC inhibition and resistance in two divergent β-CoVs, murine hepatitis virus (MHV) and MERS-CoV. We show that NHC potently inhibits WT MHV and MERS-CoV with minimal cytotoxicity. We also demonstrate that MHV ExoN proofreading activity has a limited but measurable effect on sensitivity to NHC. We observed an NHC inhibition profile consistent with a mutagenic mechanism of action featuring an accumulation of transition mutations, indicative of a high genetic barrier to resistance.

RESULTS

NHC inhibits MHV and MERS-CoV replication with minimal cytotoxicity. NHC (Fig. 1) has potent broad-spectrum antiviral activity against many RNA viral families (31–36). We first determined if NHC also inhibits CoV replication, using a dose-response

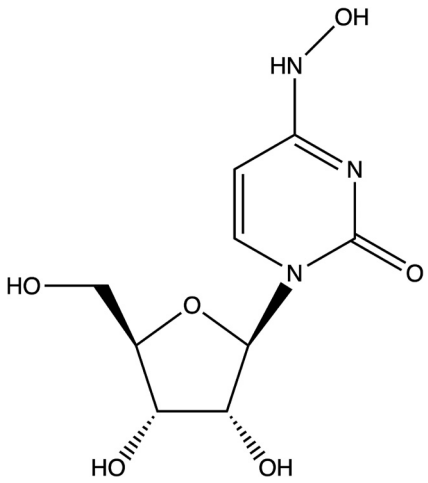

FIG 1 Chemical structure of EIDD-1931, β-D-N^4-hydroxycytidine.

experiment with two divergent β-CoVs: the model CoV MHV and the epidemically circulating zoonotic CoV MERS-CoV. NHC treatment resulted in a dose-dependent reduction in viral titers for MHV (Fig. 2A) and MERS-CoV (Fig. 2B). This inhibition resulted in 50% effective concentrations (EC_{50}s) of 0.17 μM for MHV (Fig. 2C) and 0.56 μM for MERS-CoV (Fig. 2D). We detected negligible changes in DBT-9 cell viability out to 200 μM (Fig. 2E) and 50% cytotoxic concentration (CC_{50}) values above 10 μM in Vero cells (Fig. 2F). The antiviral activity was not due to cytotoxicity, as the selectivity indexes were >1,000 for MHV and >20 for MERS-CoV. Together, these results confirm potent inhibition of β-CoVs by NHC.

The NHC inhibition profile in CoVs is consistent with mutagenesis. To better understand the mechanism through which NHC inhibits CoV replication, we performed a time of drug addition assay to determine at what point in the viral replication cycle NHC acts (40). We added 16 μM (~100 times the EC_{50}) NHC at the indicated times pre- or postinfection (p.i.) of cells with WT MHV at a multiplicity of infection (MOI) of 1 PFU/cell and quantified viral replication after a single infectious cycle. Compared to the vehicle (dimethyl sulfoxide [DMSO]) control, NHC significantly inhibited MHV replication when added at or before 6 h postinfection (Fig. 3A), suggesting that NHC acts at early stages of the viral replication cycle. We next determined the effect of NHC on MHV RNA levels and compared it to the effect on the infectious-virus titer. RNA levels were reduced by approximately 10-fold at the highest tested concentration of NHC in both MHV-infected cell monolayers (Fig. 3B) and supernatants (Fig. 3C). In contrast, the viral titer was reduced up to 5,000-fold at this concentration. We therefore calculated the ratio of infectious virus per viral RNA genome copy number normalized to the untreated control (specific infectivity) after NHC treatment and found that the specific infectivity of WT MHV was reduced in a dose-dependent manner after treatment with increasing concentrations of NHC (Fig. 3D). Together, these data are consistent with a mutagenic mechanism of NHC anti-CoV activity.

NHC treatment increases transition mutations present across the MHV genome. To directly test the effect of NHC treatment on the mutational burden, we treated WT MHV with increasing concentrations of NHC and performed full-genome next-generation sequencing (NGS) on viral populations released after a single round of infection. Our data demonstrated a dose-dependent increase in mutations present at low frequencies (<5% of the viral population) across the genome after treatment with increasing concentrations of NHC (Fig. 4A to C). Further analysis of the types of mutations introduced by NHC revealed an increase in the total number of transition mutations with increasing NHC concentrations (Fig. 4D to F). The relative proportions of G:A and C:U transitions among all observed mutations were increased by 13 to 15% in the presence of 2 μM NHC and 36 to 40% in the presence of 4 μM NHC compared

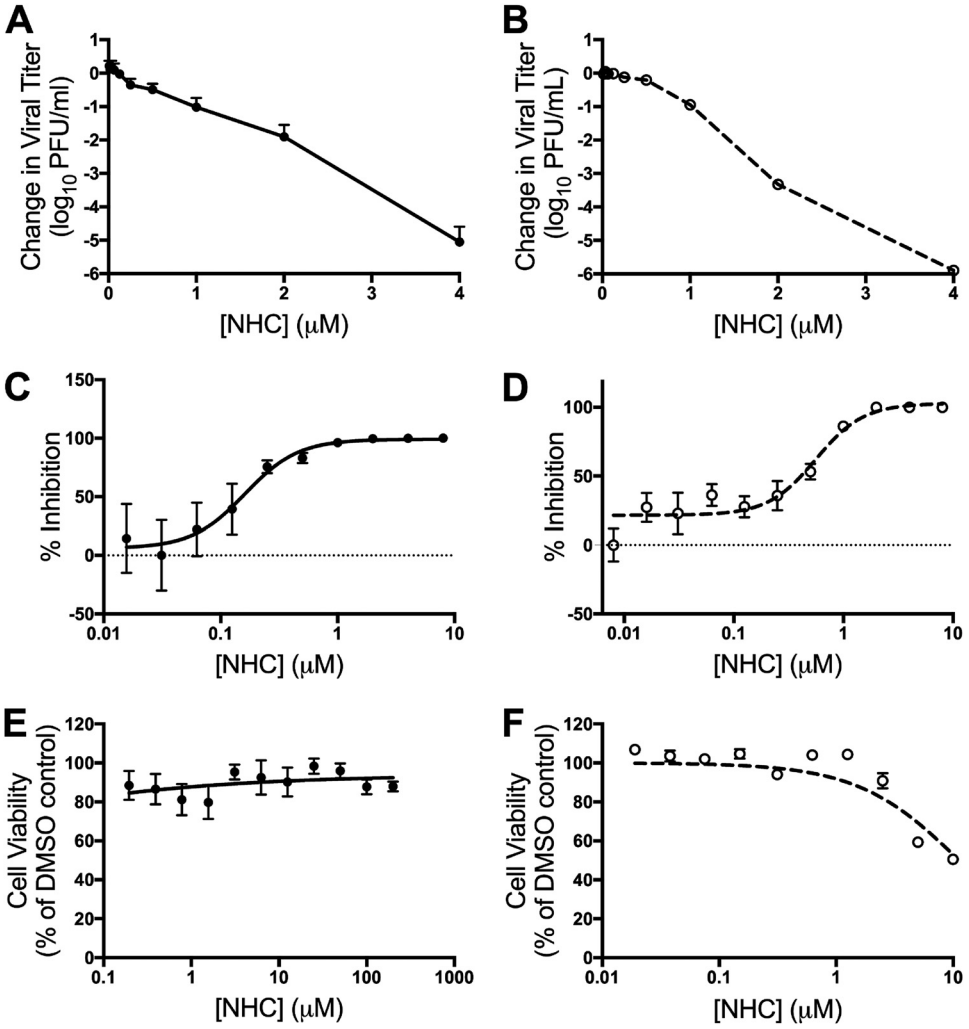

FIG 2 NHC inhibits MHV and MERS-CoV with minimal cytotoxicity. (A and B) Changes in MHV (A) and MERS-CoV (B) titers relative to vehicle control after treatment with increasing concentrations of NHC. The data represent the results of 6 independent experiments, each with 3 replicates. The error bars represent standard errors of the mean (SEM). (C) Changes in titer data from panel A, represented as percentages of that of vehicle control. WT MHV, EC_{50} = 0.17 μM. (D) Changes in titer data from panel B, represented as percentages of that of vehicle control. WT MERS-CoV, EC_{50} = 0.56 μM. (E) DBT-9 cell viability as a percentage of that of DMSO control across NHC concentrations. No cytotoxicity was detected up to 200 μM. The data represent the results of 2 independent experiments, each with 2 replicates (MHV). The error bars represent SEM. (F) Vero cell viability as a percentage of that of DMSO control across NHC concentrations. Less than 50% cytotoxicity was detected up to 10 μM. The data represent the results of 2 independent experiments, each with 3 replicates. The error bars represent SEM.

to the vehicle control (Fig. 4G and H). Conversely, the relative proportions of A:G and U:C transitions decreased with increasing NHC concentrations compared to the vehicle control (Fig. 4G and H). Together, these results demonstrate that NHC treatment during a single round of WT MHV infection causes predominantly G:A and C:U transition mutations that are detectable at low frequencies across the genome. These data further support a mutagenic mechanism of action for NHC inhibition of WT MHV.

NHC inhibition is modestly enhanced in the absence of ExoN proofreading. Mutagenic nucleoside analogues, such as RBV and 5-FU, have been ineffective at potently inhibiting WT CoVs due to the ExoN proofreading activity (26). A proofreading-deficient [ExoN(−)] MHV mutant displays increased sensitivity to previously tested nucleoside analogues, indicating that proofreading dampens inhibition by these compounds (26, 37, 38). Therefore, we tested the sensitivity of ExoN(−) MHV to NHC inhibition. Our results indicate that NHC decreases the titers of both WT and ExoN(−) MHV in a dose-dependent manner but that ExoN(−) MHV demonstrates a statistically

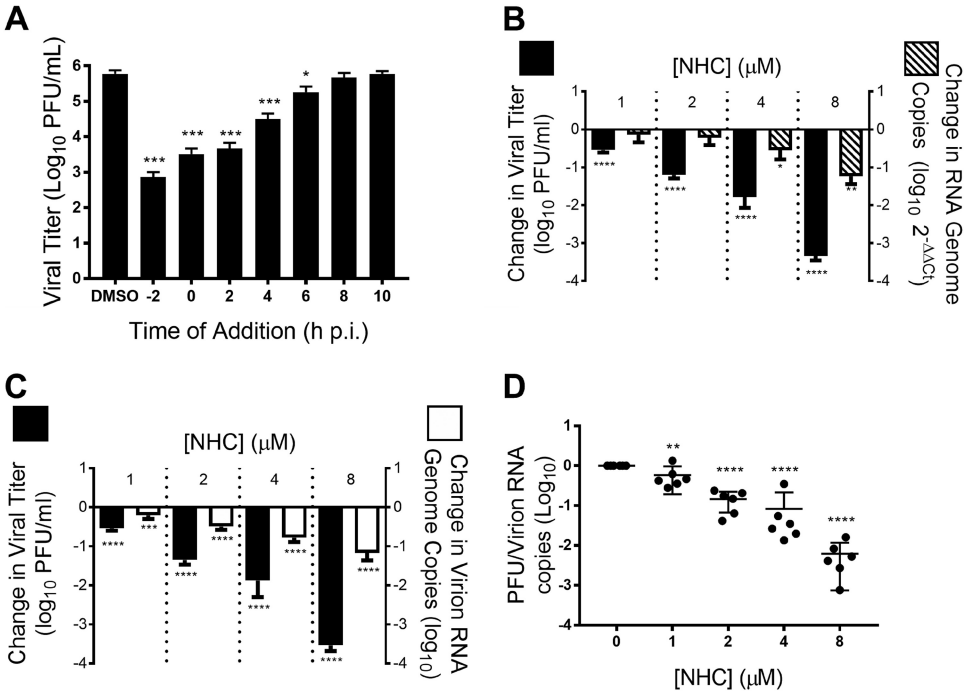

FIG 3 The NHC inhibition profile of MHV is consistent with mutagenesis. (A) Treatment with 16 μM NHC (~100 times the EC_{50}) significantly inhibits MHV replication during a single infection when added before 6 h p.i. (B) Both MHV titer and monolayer RNA copies decrease after treatment with increasing concentrations of NHC. (C) NHC treatment results in a decrease in supernatant MHV RNA. (D) Data from panel C represented as the ratio of infectious WT MHV to genomic MHV RNA present in the supernatant, or specific infectivity, normalized to that of vehicle control. NHC treatment resulted in a decrease in the specific infectivity of MHV. All the data represent the results of 2 independent experiments, each with 3 replicates. The error bars represent SEM. Statistical significance compared to DMSO control was determined by one-way analysis of variance (ANOVA) with Dunnett's *post hoc* test for multiple comparisons. *, $P < 0.05$; **; $P < 0.01$; ***, $P < 0.001$; ****, $P < 0.0001$.

significant increase in sensitivity to NHC inhibition compared to WT MHV (Fig. 5A). However, this difference is reflected in only a modest decrease in the EC_{90} (approximately 2-fold) for ExoN(−) MHV (0.72 μM) compared to WT MHV (1.59 μM) (Fig. 5B). The minimal change in sensitivity to NHC observed for ExoN(−) MHV indicates that NHC potency is only marginally affected by ExoN proofreading activity.

Passage in the presence of NHC yields low-level resistance associated with multiple transition mutations. To better understand the development and impact of NHC resistance in CoVs, we passaged two lineages of WT MHV 30 times in the presence of increasing concentrations of NHC and tested the sensitivity of passage 30 (p30) MHV populations to NHC inhibition. We found that the lineage 1 (MHV p30.1) viral population showed no change in sensitivity to NHC compared to WT MHV (Fig. 6A). However, lineage 2 (MHV p30.2) showed a decrease in sensitivity to NHC inhibition in a titer reduction assay, especially at higher concentrations of compound. We observed a modest (approximately 2-fold) increase in EC_{90} values for MHV NHC passage viruses (WT MHV, $EC_{90} = 1.53$ μM; MHV p30.1, $EC_{90} = 2.61$ μM; MHV p30.2, $EC_{90} = 2.41$ μM) (Fig. 6B). This suggests that MHV passage resulted in minimal resistance to NHC. We next sought to determine if passaging WT MHV in the presence of NHC altered the replication capacities of these viruses. We found that both lineages showed a delay in replication but ultimately reached peak titers similar to that of WT MHV (Fig. 6C). This delay in replication suggests that MHV p30 is less fit than WT MHV.

To identify mutations associated with these phenotypes after passage, we sequenced complete genomes of MHV p30.1 and MHV p30.2. Both lineages passaged in the presence NHC had accumulated over 100 consensus mutations distributed across the genomes (Fig. 6D and E; see Table S1 in the supplemental material). In comparison, a previous study reported that WT MHV accumulated only 23 total mutations after 250

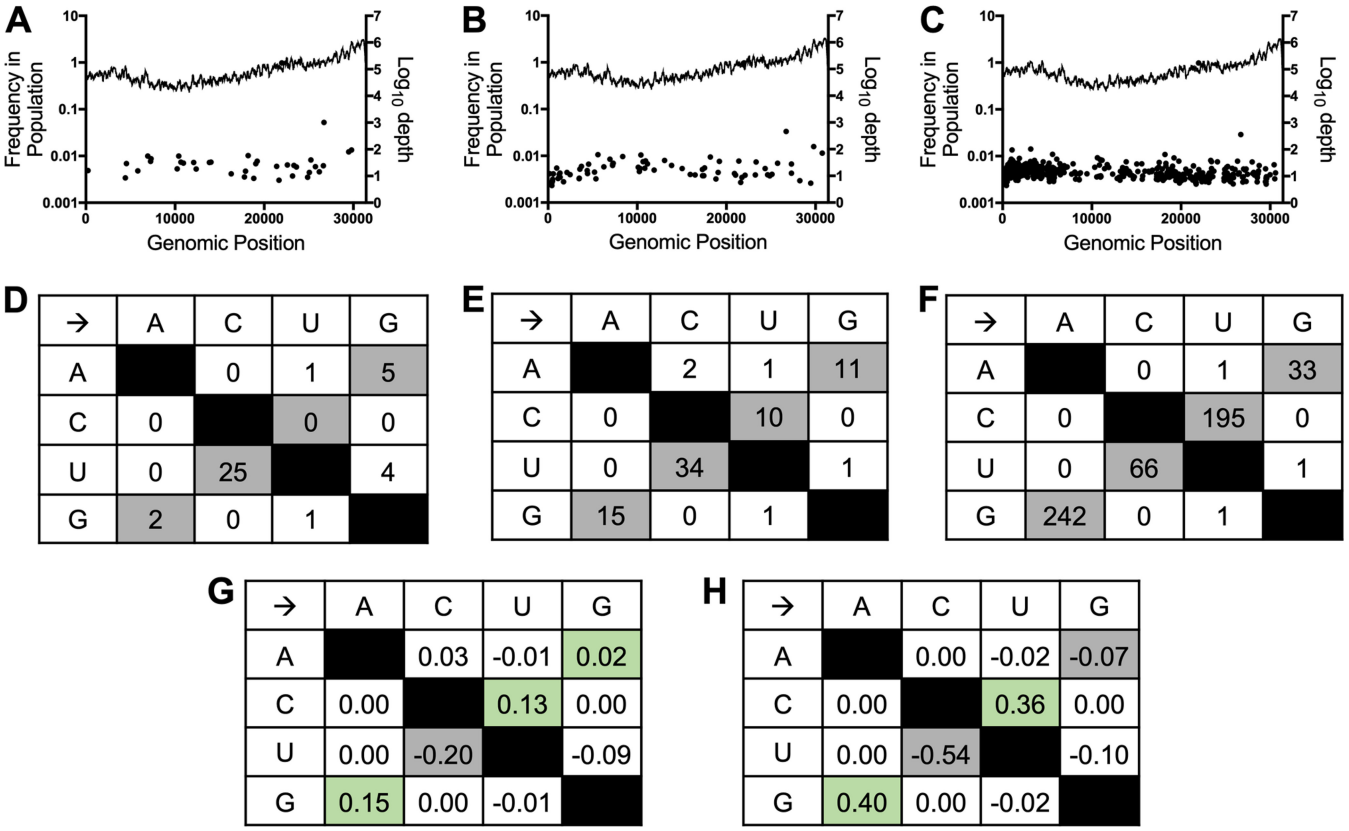

FIG 4 NHC treatment drives an increase in low-frequency G:A and C:U transition mutations in WT MHV during a single infection. (A to C) Distribution and frequencies of variants across the genome detected by NGS after vehicle treatment (A), 2 μM NHC treatment (B), or 4 μM NHC treatment (C). The $\log_{10}$ depth of coverage at each genomic position is depicted by the lines; the frequencies of individual mutations spread across the genome are represented by the dots. (D to F) Numbers of mutations in WT MHV after infection in the presence of vehicle (D), 2 μM NHC (E), or 4 μM NHC (F) presented by type. Transition mutations are shown in gray, and transversion mutations are shown in white. (G and H) Changes in relative proportions of each mutation type after treatment with 2 μM NHC (G) or 4 μM NHC (H) compared to vehicle control. The relative proportions of G:A and C:U transitions increased with increasing concentrations of NHC treatment and are indicated by green shading.

passages in the absence of drug (38). Further analysis of the p30 MHV mutational profile demonstrated that slightly more of the total mutations in both lineages were synonymous changes that did not result in an amino acid change as opposed to nonsynonymous changes, which did alter the amino acid sequence (Fig. 6F; see

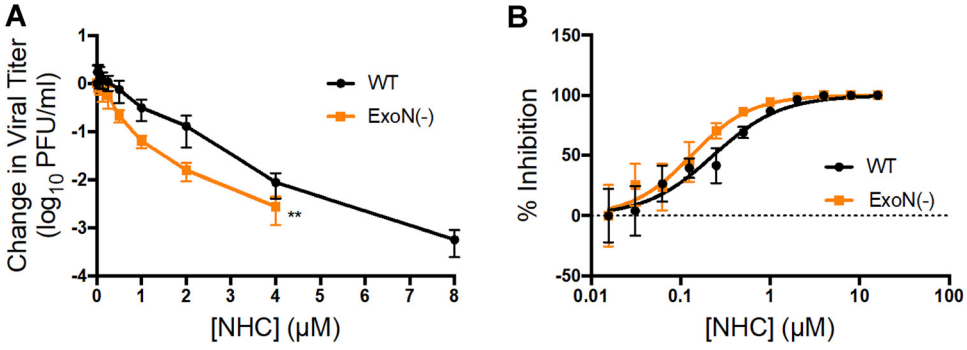

FIG 5 Sensitivity of ExoN(−) MHV to inhibition by NHC. (A) Changes in viral titers for WT MHV and ExoN(−) MHV relative to vehicle control after treatment with NHC. ExoN(−) MHV is more sensitive to NHC than WT MHV. The data represent the results of 3 independent experiments, each with 3 replicates. The error bars represent SEM. Statistical significance compared to WT MHV was determined by a Wilcoxon test. **, $P < 0.01$. (B) Changes in viral titer data from panel A represented as a percentage of that in vehicle control. WT, EC_{90} = 1.59 μM; ExoN(−), EC_{90} = 0.72 μM. ExoN(−) MHV is approximately 2-fold more sensitive to NHC than WT MHV.

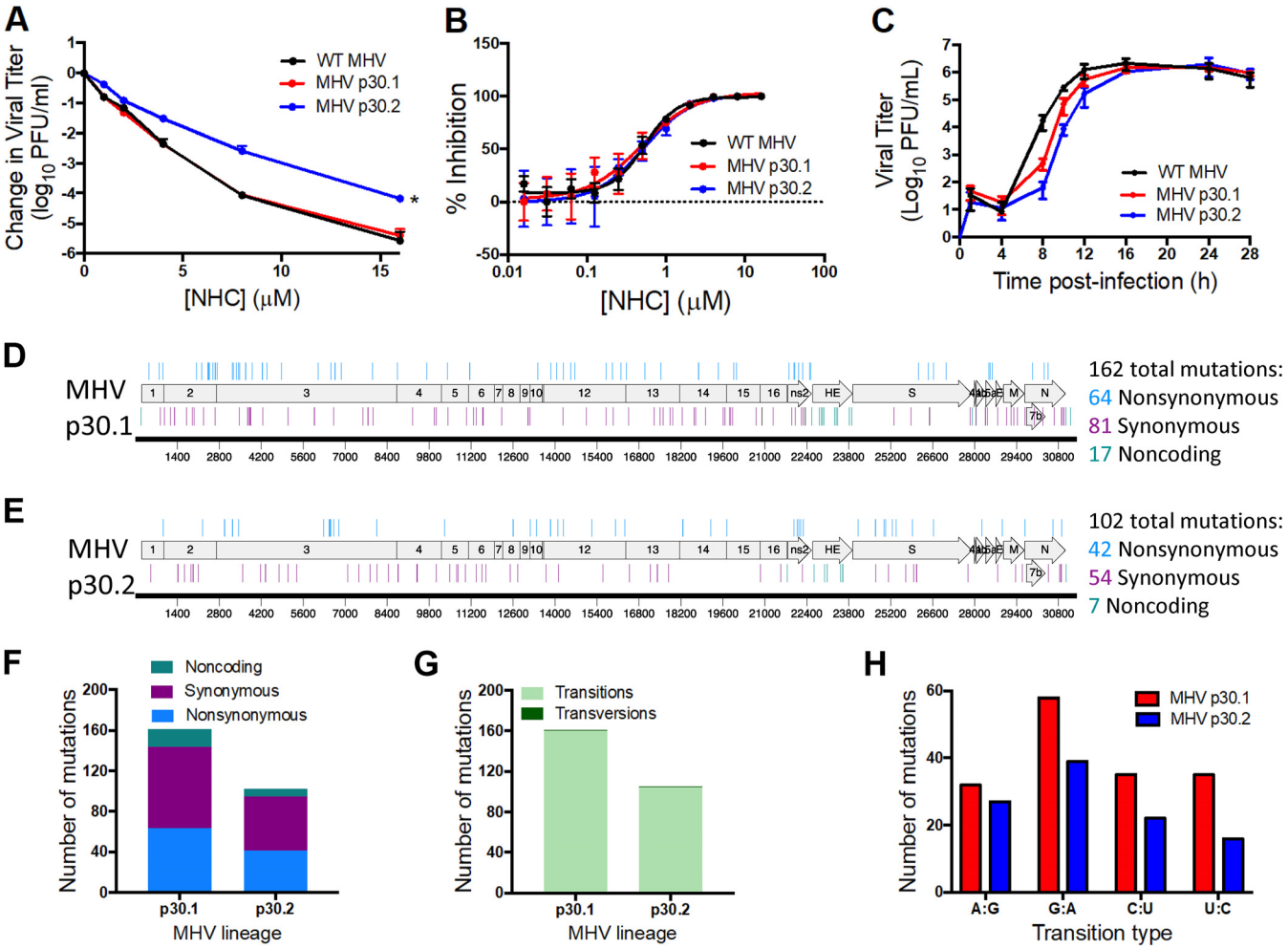

FIG 6 Resistance and mutational profiles of MHV after 30 passages in the presence of NHC. (A) Changes in viral titers for WT MHV, MHV p30.1, and MHV p30.2 relative to vehicle controls after treatment with NHC. MHV NHC p30.2 was less sensitive to NHC than WT MHV, while MHV p30.1 showed no change in sensitivity. The data represent the results of 2 independent experiments, each with 3 replicates. The error bars represent SEM. Statistical significance compared to WT MHV was determined by ratio paired *t* test. *, $P < 0.05$. (B) Changes in viral titer data from panel A represented as percentages of that of vehicle control. WT MHV, $EC_{90} = 1.53$ μM; MHV p30.1, $EC_{90} = 2.61$ μM; MHV p30.2, $EC_{90} = 2.41$ μM. (C) Replication kinetics of NHC passage viruses. MHV p30.1 and p30.2 were delayed in replication compared to WT MHV but ultimately reached similar peak titers. The data represent the results of 2 independent experiments, each with 3 replicates. The error bars represent standard deviations (SD). (D) MHV p30.1 accumulated a total of 162 consensus mutations across the genome that were detectable by Sanger sequencing. Of these mutations, 81 were synonymous, 64 were nonsynonymous, and 17 were noncoding. (E) MHV p30.2 accumulated 102 total mutations across the genome. Of these mutations, 54 were synonymous, 42 were nonsynonymous, and 7 were noncoding. (F) Each lineage accumulated more synonymous changes than nonsynonymous or noncoding changes over passage. (G) Breakdown of transition and transversion mutations present in each lineage after passage. MHV p30.1 and p30.2 mutations were predominantly transitions. (H) Breakdown of the types of transition mutations present in each lineage across passage. G:A transitions were the most abundant for both MHV p30.1 and p30.2.

Table S1). Additionally, the vast majority of mutations in both lineages were transition mutations resulting in a purine-to-purine or pyrimidine-to-pyrimidine change (Fig. 6G). Both lineages contained only two transversion mutations resulting in a purine-to-pyrimidine or pyrimidine-to-purine change. Though all possible transition mutation types were detected in both viral-lineage populations, the majority in both passage lineages were G:A transitions (Fig. 6H), which is consistent with the MHV NGS data (Fig. 4). To determine if the mutational profile at p30 was consistent with an earlier passage, we analyzed the whole genomes of both lineages 1 and 2 at p19. Both lineages demonstrated fewer mutations at p19 than at p30, but the profiles of synonymous versus nonsynonymous changes and the transition mutations were similar (see Fig. S1 and Table S2 in the supplemental material).

To determine whether the lack of robust resistance to NHC was broadly applicable across β-CoVs, we assessed the capacity of MERS-CoV to evolve resistance to NHC. As

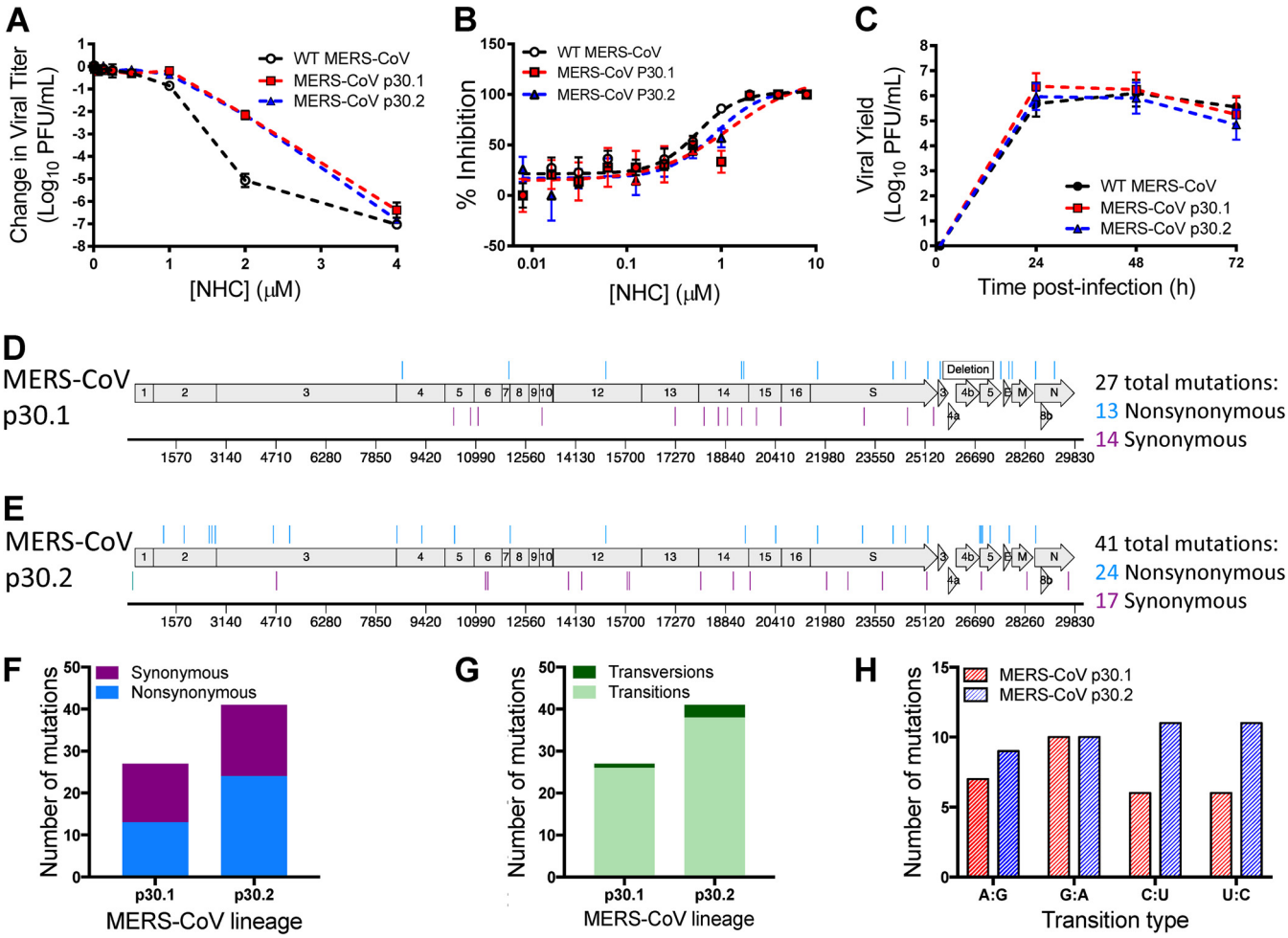

FIG 7 Resistance and mutational profiles of MERS-CoV after 30 passages in the presence of NHC. (A) Changes in viral titers relative to vehicle controls after treatment with NHC for WT MERS-CoV passaged 30 times in the absence of drug, MERS-CoV p30.1, and MERS-CoV p30.2 relative to vehicle controls after treatment with NHC. Both MERS-CoV p30.1 and p30.2 were less sensitive to NHC than WT MERS-CoV. The data represent the results of 2 independent experiments, each with 3 replicates. The error bars represent SEM. (B) Changes in viral titer data from panel A represented as percentages of that of vehicle control. WT MERS-CoV, EC_{90} = 1.31 μM; MERS-CoV p30.1, EC_{90} = 3.04 μM; MERS-CoV p30.2, EC_{90} = 2.12 μM. (C) Replication kinetics of NHC passage viruses. WT MERS-CoV, MERS-CoV p30.1, and MERS-CoV p30.2 replicated with similar kinetics and reached similar peak titers. The data represent the results of 2 independent experiments, each with 3 replicates. The error bars represent SEM. (D) MERS-CoV p30.1 accumulated 27 total mutations across the genome. Of these mutations, 14 were synonymous and 13 were nonsynonymous. (E) MERS-CoV p30.2 accumulated 41 total mutations. Of these mutations, 17 were synonymous and 24 were nonsynonymous. (F) Both MERS-CoV p30.1 and p30.2 accumulated similar numbers of nonsynonymous and synonymous changes during passage. (G) MERS-CoV p30.1 and p30.2 acquired predominantly transitions. (H) Types of transition mutations present in each lineage across passage. MERS-CoV p30.1 acquired more G:A transitions, whereas MERS-CoV p30.2 acquired similar numbers of each transition type.

with MHV, we passaged two lineages of MERS-CoV 30 times in the presence of increasing concentrations of NHC and tested the sensitivities of the lineages to inhibition by NHC. Compared to WT MERS-CoV passaged in the absence of drug, both MERS-CoV NHC p30.1 and p30.2 exhibited decreased sensitivity to NHC inhibition (Fig. 7A). This correlated with modestly increased EC_{90} values for the passage lineages (WT MERS-CoV, EC_{90} = 1.31 μM; MERS-CoV p30.1, EC_{90} = 3.04 μM; MERS-CoV p30.2, EC_{90} = 2.12 μM) (Fig. 7B), corresponding to approximately 2-fold resistance. Similar to MHV, we observed no substantial shift in the dose-response curve for MERS-CoV, indicating minimal acquired resistance. NHC p30 viruses replicated similarly to WT p30 MERS-CoV (Fig. 7C). We sequenced both lineages of the MERS-CoV p30 population and detected 27 consensus mutations in MERS-CoV NHC p30.1 (Fig. 7D; see Table S3 in the supplemental material) and 41 consensus mutations in MERS-CoV NHC p30.2 (Fig. 7E; see Table S3) that were randomly distributed across the genome. Both MERS-CoV NHC p30.1 and MERS-CoV NHC p30.2 accumulated nonsynonymous and synonymous mu-

tations in roughly equal proportions (Fig. 7F). As in MHV, the mutations detected in MERS-CoV p30 lineages were predominantly transition mutations (Fig. 7G). Further analysis of these mutations revealed that the predominant type of transition was lineage dependent. The majority of transition mutations in MERS-CoV NHC p30.1 were G:A transitions, as was observed in both p30 MHV lineages, whereas MERS-CoV NHC p30.2 contained similar numbers of each type (Fig. 7H). These results indicate that MERS-CoV can achieve low-level resistance to NHC and that development of resistance is associated with the accumulation of multiple transition mutations. Together, our data suggest NHC acts as a mutagen and that it poses a high genetic barrier to resistance for β-CoVs.

DISCUSSION

In this study, we demonstrate that NHC potently inhibits the divergent β-CoVs MHV and MERS-CoV. Our data are consistent with a virus-mutagenic mechanism of action, as evidenced by a decrease in specific infectivity and an increase in G:A and C:U transition mutations present at low frequencies across the genome after treatment with NHC. We also demonstrate that robust resistance to NHC is difficult to achieve in both MHV and MERS-CoV. Both WT MHV and ExoN(−) MHV are sensitive to NHC inhibition, suggesting that NHC is able to overcome ExoN-mediated proofreading to inhibit WT CoVs and that it interacts with CoVs differently than other previously tested nucleoside analogues.

Utility of the broad-spectrum antiviral NHC as a pan-CoV therapeutic. Early work with NHC focused on the mutagenic effects of the compound in multiple bacterial systems (39, 41, 42). More recently, the antiviral properties of the compound have been reported for multiple RNA viruses, including chikungunya virus, Venezuelan equine encephalitis virus, respiratory syncytial virus, hepatitis C virus, norovirus, influenza A and B viruses, and Ebola virus (31–36). NHC has also been shown to potently inhibit SARS-CoV and HCoV-NL63 (43, 44), suggesting potential utility in treating CoV infections (17). Based on previous studies, NHC appears to primarily inhibit viral replication by mutagenesis (31, 34). Serial passaging in the presence of NHC led to low-level resistance for VEEV, but no detectable resistance for RSV, IAV, or bovine viral diarrhea virus, indicating a high barrier to resistance (31, 34, 36). Consistent with the previous studies, we demonstrated that NHC is mutagenic in CoVs and that serial passaging yields low-level, approximately 2-fold resistance. Low-level resistance has also been observed for remdesivir, another nucleoside analogue that potently inhibits CoVs. Approximately 6-fold resistance to remdesivir is conferred by two mutations in the CoV RNA-dependent RNA polymerase (RdRp) (37). This study further expands the known antiviral spectrum of NHC to include MHV and MERS-CoV, two genetically divergent β-CoVs, and supports NHC development as a broad-spectrum CoV antiviral.

NHC inhibition may circumvent ExoN-mediated proofreading. NHC is the first mutagenic nucleoside analogue demonstrated to potently inhibit proofreading-intact CoVs. Previous studies have demonstrated that viruses lacking ExoN proofreading activity [ExoN(−) viruses] are more sensitive to inhibition by nucleoside analogues, especially RBV and 5-FU (26, 37, 38, 45). This increased sensitivity has been attributed to the inability of ExoN(−) viruses to efficiently remove incorrect nucleosides (46). However, we observed a minimal change in NHC sensitivity between WT MHV and ExoN(−) MHV, especially by EC_{90}. This suggests that NHC interacts with the CoV replicase differently than other previously tested nucleoside analogues. One explanation is that NHC may evade removal by the proofreading ExoN. Studies investigating nucleosides that inhibit DNA viruses have suggested an inability of the viral exonuclease to efficiently excise some nucleoside analogues (47, 48). Further, a previous study suggested that the T4 DNA exonuclease activity was incapable of removing NHC (49). While the SARS-CoV ExoN efficiently removes 3′-terminal mismatches regardless of type (46, 50), the effect of NHC on this activity has not been investigated. Interestingly, mismatches readily observed during single-nucleotide elongation by the SARS-CoV polymerase in the absence of drugs correspond to mismatches that would lead to the G:A and C:U transitions observed after NHC treatment (46). This suggests that the CoV

polymerase could be naturally more prone to make these types of errors, which are then magnified by NHC. This could lead to a scenario where ExoN cannot prevent dipping below the error threshold, ultimately resulting in lethal mutagenesis and similar inhibition of both WT MHV and ExoN(−) MHV (51).

Several nucleosides, including the mutagenic RBV, have multiple demonstrated mechanisms other than direct incorporation into the genome (52, 53). Thus, another explanation for the unique potency of NHC in the presence of an active proofreading ExoN is that it may inhibit viral replication by additional mechanisms beyond mutagenesis. Indeed, previous reports have suggested that NHC may also interfere with the RNA secondary structure or virion release to cause inhibition (31, 36). Further, exogenous C or U in the presence of NHC could rescue viral replication in HCV, chikungunya virus, RSV, and influenza A virus (32, 34, 36), indicating that NHC competes with exogenous nucleosides at some stage prior to viral inhibition. These results raise the possibility that NHC could inhibit a process that results in similar inhibition of these viruses by a mechanism unrelated to ExoN. Thus, future studies will be important to investigate the role of proofreading in NHC inhibition of CoVs to shed light on the intricacies of NHC inhibition of the CoV replication complex.

NHC mutagenesis may hinder emergence of robust resistance to NHC. The decrease in specific infectivity, along with the accumulation of transitions across the CoV genome, supports a mutagenic mechanism of action for NHC in CoVs. NHC resistance in CoVs was modest and difficult to achieve, as we obtained approximately 2-fold resistance after 30 passages. Resistance was associated with multiple mutations. Interestingly, MERS-CoV accumulated fewer mutations over 30 passages than MHV. While differences in viral mutation rates could be the driver of this difference, previous studies have suggested that MHV does not have a higher mutation rate than MERS-CoV (54–56). The differences in mutation accumulation between MHV and MERS-CoV may be a product of different passage conditions. While MHV was passaged with a consistent transfer volume, MERS-CoV passage volumes were adjusted over time to sustain viral replication under escalating selection for drug resistance. The constant-volume passaging conditions may have more severely bottlenecked MHV populations and fixed more mutations in the genome than the variable-volume passaging conditions applied to MERS-CoV (57). Alternatively, this difference could also reflect a difference in mutational robustness of the MHV and MERS-CoV genomes, though this proposition needs to be investigated further (58, 59). While a portion of the mutations that accumulated during passage likely contribute to NHC resistance, mutations in proteins dispensable for viral replication in cell culture, such as ns2 and nsp2, may be merely tolerated because of their limited effect on viral fitness in the context of our passage conditions (60–62). Few common mutations arose in both MHV and MERS-CoV passage series (see Tables S1 to S3), suggesting that multiple pathways to low-level NHC resistance exist in CoVs. Interestingly, for both MHV and MERS-CoV, the p30 lineage that demonstrated a greater change in sensitivity to NHC was the lineage that had fewer overall mutations (Fig. 6 and 7). Both MHV passage lineages replicated less well than WT MHV, suggesting that the accumulation of mutations during passage may negatively impact viral fitness and the ability of MHV to evolve robust resistance to NHC. Further, the MHV lineage that did not result in changed sensitivity to NHC by p30 (MHV p30.1) had fewer mutations present at consensus by p19 than the other lineage (see Fig. S1). Thus, it is possible that the accumulation of deleterious mutations counteracts the potential benefits of resistance mutations (63). If this is the case, mutations promoting NHC resistance would need to arise early during passage to help mitigate the accumulation of excess deleterious mutations. Alternatively, the inability to evade inhibition by NHC may lead to the accumulation of a greater number of NHC-associated transitions and ultimately a higher mutational burden that may impact viral fitness (64, 65). Together, our results support the hypothesis that establishment of resistance to NHC in CoVs requires a delicate balance of resistance-promoting mutations, viral fitness, and accumulation of deleterious mutations. Thus, defining the roles of individ-

ual NHC resistance-associated mutations will be an important goal for future studies. Overall, our results support further development of NHC as a broad-spectrum antiviral for treatment of CoV infections and contribute new insights into important aspects of CoV replication.

MATERIALS AND METHODS

Cell culture. Murine astrocytoma delayed brain tumor (DBT) (66) and Vero (ATCC CCL-81) cells were maintained at 37°C in Dulbecco's modified Eagle medium (DMEM) (Gibco) supplemented with 10% fetal bovine serum (FBS) (Invitrogen), 1% penicillin and streptomycin (Gibco), and 0.1% amphotericin B (Corning).

Viruses. All work with MHV was performed using the recombinant WT strain MHV-A59 (GenBank accession number AY910861 [67]). MERS-CoV stocks were generated from cDNA clones (GenBank accession number JX869059 [68]).

Compounds and cell viability studies. NHC was synthesized at the Emory Institute for Drug Development and prepared as a 20 mM stock solution in DMSO. Cell viability was assessed using CellTiter-Glo (Promega) in 96-well plates according to the manufacturer's instructions. DBT and Vero cells were incubated with the indicated concentrations of compound at 37°C for 24 h (DBT) or 48 h (Vero). Cell viability was determined using a Veritas Microplate luminometer (Promega) or GloMax (Promega), with values normalized to those of vehicle-treated cells.

Nucleoside analogue sensitivity studies and generation of EC_{50} curves. Subconfluent monolayers of DBT cells were infected with MHV at an MOI of 0.01 PFU per cell for 1 h at 37°C. The inoculum was removed and replaced with medium containing the indicated compound concentration. Cell supernatants were harvested 24 h postinfection. Titers were determined by plaque assay as described previously (69). Subconfluent monolayers of Vero cells were infected at an MOI of 0.01 PFU/cell of MERS-CoV. After virus adsorption for 30 min at 37°C, the inoculum was removed. The cells were washed with PBS and incubated with medium containing the indicated concentrations of NHC or DMSO (vehicle control). After 48 h, the supernatant was collected and titers were determined by plaque assay as described previously (70). EC_{50} and EC_{90} values and curves were generated using the nonlinear regression curve fit in GraphPad (La Jolla, CA) Prism software.

Time of drug addition assay. Subconfluent monolayers of DBT cells were treated with medium containing DMSO or 16 μM NHC (~100 times the EC_{50}) at the indicated times pre- or postinfection. The cells were infected with WT MHV at an MOI of 1 PFU/cell for 1 h at 37°C. The virus inoculum was removed and replaced with fresh medium. Culture supernatant was harvested 12 h postinfection, and the viral titer was determined by plaque assay.

Quantification of viral genomic RNA. Subconfluent DBT cells were infected with WT MHV at an MOI of 0.01 PFU/cell. The inoculum was removed after 1 h of incubation at 37°C, and medium containing the indicated concentration of NHC was added. Total RNA from cells and supernatant RNA were harvested using TRIzol reagent (Invitrogen) after 20 h. Both total RNA and supernatant RNA were extracted by phase separation. Total RNA was purified by ethanol precipitation, and supernatant RNA was purified using a PureLink RNA minikit (Invitrogen) according to the manufacturer's protocol. Total RNA was reverse transcribed using SuperScript III (Invitrogen) to generate cDNA, which was quantified by quantitative PCR (qPCR) as previously described (26). Data are presented as $2^{-\Delta\Delta CT}$, where $\Delta\Delta C_T$ denotes the change in the threshold cycle for the viral target (nsp10) normalized to the control (glyceraldehyde-3-phosphate dehydrogenase [GAPDH]) before and after drug treatment. The supernatant RNA was quantified using one-step quantitative reverse transcriptase PCR (qRT-PCR) as previously described (45). The data are presented as the fold change in genome RNA copies normalized to vehicle control.

Determination of specific infectivity. Subconfluent DBT cells were infected with WT MHV at an MOI of 0.01 PFU/cell. The inoculum was removed after 1 h of incubation at 37°C, and medium containing the indicated concentration of NHC was added. Supernatant RNA was harvested using the TRIzol reagent (Invitrogen) after 20 h, followed by extraction and quantification as described above. The viral titer was determined by plaque assay. The specific infectivity was calculated as the number of PFU divided by the supernatant genome RNA copy number. This ratio was then normalized to that of the vehicle control.

NGS studies. Subconfluent DBT cells were infected with WT MHV at an MOI of 0.01 PFU/cell and treated with the indicated concentrations of NHC. The supernatant was collected 24 h postinfection. Purified viral RNA was submitted to Genewiz (South Plainfield, NJ) for library preparation and sequencing. Briefly, after quality controls, viral RNAs were randomly fragmented using heat. Libraries were prepared and sequenced on the Illumina HiSeq platform.

Genewiz performed base calling and read demultiplexing. Trimmomatic was used to trim adapter contaminants and reads shorter than 36 bp and to filter low-quality bases (Q score $<$ 30) (71). The paired-end fastq reads were then aligned with the MHV genome using Bowtie2 to generate a SAM file (72). SAMtools was used to process the resultant alignment file and to calculate the coverage depth at each nucleotide, generating a sorted and indexed BAM file. LoFreq was used to call substitution variants, including low-frequency variants, and to generate a variant file (73). The Bash shell and Excel were used to further process and analyze the resultant vcf file. A frequency of 0.001 was used as a cutoff for variants, consistent with previous reports (74). Absolute numbers of mutations are reported for each NHC treatment. The percentage of the total mutations for each specific mutation type was calculated using these numbers. The difference in percentage for each class of mutation after treatment compared with vehicle control is referred to as the relative proportion of these mutations.

MHV population passage in the presence of NHC. WT MHV was passaged in triplicate in increasing concentrations of NHC from 1 μM to a maximum of 5 μM. Infection was initiated for passage 1 at an MOI of 0.1 PFU/cell. Viral supernatants were harvested from each viral lineage and frozen when the cell monolayer demonstrated 80% cytopathic effect (CPE) or after 24 h. A constant volume of 16 μl was used to initiate subsequent passages. All three lineages were maintained until passage 16, when lineage 3 demonstrated no visible CPE upon multiple attempts at varying concentrations. Lineages 1 and 2 were maintained until passage 30. After each passage, total RNA was harvested from infected cell monolayers using the TRIzol reagent. Viral RNA was extracted from passage 19 and passage 30 samples and reverse transcribed using SuperScript III, followed by generation of 12 PCR amplicons to cover the whole genome. Dideoxy amplicon sequencing was performed by Genewiz and analyzed to identify mutations present at greater than 50% of the total using MacVector. Viral mutation maps depicting the identified mutations were generated using MacVector.

MERS-CoV population passage in the presence of NHC. Three parallel independent passage series of WT MERS-CoV were performed on Vero cells in the presence of gradually increasing concentrations of NHC up to a maximum concentration of 6.5 μM to select for drug-resistant mutant viruses. Virus adaptation to NHC-supplemented complete culture medium was assessed by monitoring the progression of characteristic MERS-CoV CPE. The volumes of transferred culture supernatants were adjusted empirically to balance continuous selective pressure against culture extinction. Each of triplicate lineages in the MERS-CoV passage experiment was sustained through passage 30. However, the third lineage was severely impaired in replication and was excluded from further analysis. Total infected-cell MERS-CoV RNA purified from monolayers infected with terminal-passage (p30) culture supernatant was used to generate RT-PCR products for consensus Sanger sequencing of the complete viral genome (Genewiz). Changes in passaged virus nucleotide and deduced amino acid sequences were identified via alignment with the WT parental virus genomic sequence using MacVector.

Virus replication assays. Subconfluent monolayers of DBT (MHV) or Vero (MERS-CoV) cells were infected with WT or NHC-passaged viral populations at an MOI of 0.01 PFU/cell for 1 h (MHV) or 30 min (MERS-CoV). Inocula were removed, and the cells were washed with PBS before addition of prewarmed medium. Supernatants were harvested at the indicated times postinfection, and titers were determined by plaque assay.

Statistics. Statistical tests were performed using GraphPad (La Jolla, CA) Prism 7 software as described in the respective figure legends.

SUPPLEMENTAL MATERIAL

Supplemental material for this article may be found at https://doi.org/10.1128/JVI.01348-19.

SUPPLEMENTAL FILE 1, XLSX file, 0.02 MB.

SUPPLEMENTAL FILE 2, XLSX file, 0.01 MB.

SUPPLEMENTAL FILE 3, XLSX file, 0.01 MB.

SUPPLEMENTAL FILE 4, PDF file, 0.2 MB.

ACKNOWLEDGMENTS

We thank members of the Denison laboratory for thoughtful discussions regarding this work.

This work was supported by Antiviral Drug Discovery and Development Center grants U19AI109680 and U19AI142759 (M.R.D. and R.S.B.); National Institutes of Health grant HHSN272201500008C (G.R.P.); and National Institutes of Health grants T32 AI112541 (M.L.A.), F31AI133952 (M.L.A.), and T32GM065086 (J.G.).

REFFERENCES

1. Ksiazek TG, Erdman D, Goldsmith CS, Zaki SR, Peret T, Emery S, Tong S, Urbani C, Comer JA, Lim W, Rollin PE, Dowell SF, Ling A-E, Humphrey CD, Shieh W-J, Guarner J, Paddock CD, Rota P, Fields B, DeRisi J, Yang J-Y, Cox N, Hughes JM, DeLuc JW, Bellini WJ, Anderson LJ. 2003. A novel coronavirus associated with severe acute respiratory syndrome. N Engl J Med 348:1953–1966. https://doi.org/10.1056/NEJMoa030781.
2. Zaki AM, van Boheemen S, Bestebroer TM, Osterhaus A, Fouchier R. 2012. Isolation of a novel coronavirus from a man with pneumonia in Saudi Arabia. N Engl J Med 367:1814–1820. https://doi.org/10.1056/NEJMoa1211721.
3. Nassar MS, Bakrebah MA, Meo SA, Alsuabeyl MS, Zaher WA. 2018. Global seasonal occurrence of Middle East respiratory syndrome coronavirus (MERS-CoV) infection. Eur Rev Med Pharmacol Sci 22:3913–3918. https://doi.org/10.26355/eurrev_201806_15276.
4. McIntosh K, Kapikian AZ, Turner HC, Hartley JW, Parrott RH, Chanock RM. 1970. Seroepidemiologic studies of coronavirus infection in adults and children. Am J Epidemiol 91:585–592. https://doi.org/10.1093/oxfordjournals.aje.a121171.
5. Gaunt ER, Hardie A, Claas ECJ, Simmonds P, Templeton KE. 2010. Epidemiology and clinical presentations of the four human coronaviruses 229E, HKU1, NL63, and OC43 detected over 3 years using a novel multiplex real-time PCR method. J Clin Microbiol 48:2940–2947. https://doi.org/10.1128/JCM.00636-10.
6. Walsh EE, Shin JH, Falsey AR. 2013. Clinical impact of human coronaviruses 229E and OC43 infection in diverse adult populations. J Infect Dis 208:1634–1642. https://doi.org/10.1093/infdis/jit393.
7. Menachery VD, Yount BL, Debbink K, Agnihothram S, Gralinski LE, Plante JA, Graham RL, Scobey T, Ge X-Y, Donaldson EF, Randell SH, Lanzavecchia A, Marasco WA, Shi Z-L, Baric RS. 2015. A SARS-like cluster of circulating bat coronaviruses shows potential for human emergence. Nat Med 21:1508–1513. https://doi.org/10.1038/nm.3985.
8. Menachery VD, Yount BL, Jr, Sims AC, Debbink K, Agnihothram SS, Gralinski LE, Graham RL, Scobey T, Plante JA, Royal SR, Swanstrom J, Sheahan TP, Pickles RJ, Corti D, Randell SH, Lanzavecchia A, Marasco WA, Baric RS. 2016. SARS-like WIV1-CoV poised for human emer-

gence. Proc Natl Acad Sci U S A 113:3048–3053. https://doi.org/10.1073/pnas.1517719113.
9. Anthony SJ, Gilardi K, Menachery VD, Goldstein T, Ssebide B, Mbabazi R, Navarrete-Macias I, Liang E, Wells H, Hicks A, Petrosov A, Byarugaba DK, Debbink K, Dinnon KH, Scobey T, Randell SH, Yount BL, Cranfield M, Johnson CK, Baric RS, Lipkin WI, Mazet J. 2017. Further evidence for bats as the evolutionary source of Middle East respiratory syndrome coronavirus. mBio 8:e00373-17. https://doi.org/10.1128/mBio.00373-17.
10. Yang Y, Du L, Liu C, Wang L, Ma C, Tang J, Baric RS, Jiang S, Li F. 2014. Receptor usage and cell entry of bat coronavirus HKU4 provide insight into bat-to-human transmission of MERS coronavirus. Proc Natl Acad Sci U S A 111:12516–12521. https://doi.org/10.1073/pnas.1405889111.
11. Twu S-J, Chen T-J, Chen C-J, Olsen SJ, Lee L-T, Fisk T, Hsu K-H, Chang S-C, Chen K-T, Chiang I-H, Wu Y-C, Wu J-S, Dowell SF. 2003. Control measures for severe acute respiratory syndrome (SARS) in Taiwan. Emerg Infect Dis 9:718–720. https://doi.org/10.3201/eid0906.030283.
12. Balkhy HH, Alenazi TH, Alshamrani MM, Baffoe-Bonnie H, Arabi Y, Hijazi R, Al-Abdely HM, El-Saed A, Johani Al S, Assiri AM, bin Saeed A. 2016. Description of a hospital outbreak of Middle East respiratory syndrome in a large tertiary care hospital in Saudi Arabia. Infect Control Hosp Epidemiol 37:1147–1155. https://doi.org/10.1017/ice.2016.132.
13. Park GE, Ko J-H, Peck KR, Lee JY, Lee JY, Cho SY, Ha YE, Kang C-I, Kang J-M, Kim Y-J, Huh HJ, Ki C-S, Lee NY, Lee JH, Jo IJ, Jeong B-H, Suh GY, Park J, Chung CR, Song J-H, Chung DR. 2016. Control of an outbreak of Middle East respiratory syndrome in a tertiary hospital in Korea. Ann Intern Med 165:87–88. https://doi.org/10.7326/M15-2495.
14. Cheng VCC, Chan JFW, To KKW, Yuen KY. 2013. Clinical management and infection control of SARS: lessons learned. Antiviral Res 100:407–419. https://doi.org/10.1016/j.antiviral.2013.08.016.
15. Stockman LJ, Bellamy R, Garner P. 2006. SARS: systematic review of treatment effects. PLoS Med 3:e343. https://doi.org/10.1371/journal.pmed.0030343.
16. Arabi Y, Shalhoub S, Mandourah Y, Al-Hameed F, Al-Omari A, Qasim Al E, Jose J, Alraddadi B, Almotairi A, Khatib Al K, Abdulmomen A, Qushmaq I, Sindi AA, Mady A, Solaiman O, Al-Raddadi R, Maghrabi K, Ragab A, Mekhlafi Al GA, Balkhy HH, Harthy Al A, Kharaba A, Gramish JA, Al-Aithan AM, Al-Dawood A, Merson L, Hayden FG, Fowler R, Saudi Critical Care Trials Group. 25 June 2019. Ribavirin and interferon therapy for critically ill patients with the Middle East respiratory syndrome: a multicenter observational study. Clin Infect Dis https://doi.org/10.1093/cid/ciz544.
17. De Clercq E. 2006. Potential antivirals and antiviral strategies against SARS coronavirus infections. Expert Rev Anti Infect Ther 4:291–302. https://doi.org/10.1586/14787210.4.2.291.
18. Zumla A, Chan JFW, Azhar EI, Hui DSC, Yuen K-Y. 2016. Coronaviruses—drug discovery and therapeutic options. Nat Rev Drug Discov 15:327–347. https://doi.org/10.1038/nrd.2015.37.
19. Adedeji AO, Sarafianos SG. 2014. Antiviral drugs specific for coronaviruses in preclinical development. Curr Opin Virol 8:45–53. https://doi.org/10.1016/j.coviro.2014.06.002.
20. Clercq ED. 2004. Antivirals and antiviral strategies. Nat Rev Microbiol 2:704–720. https://doi.org/10.1038/nrmicro975.
21. De Clercq E, Li G. 2016. Approved antiviral drugs over the past 50 years. Clin Microbiol Rev 29:695–747. https://doi.org/10.1128/CMR.00102-15.
22. Jordheim LP, Durantel D, Zoulim F, Dumontet C. 2013. Advances in the development of nucleoside and nucleotide analogues for cancer and viral diseases. Nat Rev Drug Discov 12:447–464. https://doi.org/10.1038/nrd4010.
23. Deval J. 2009. Antimicrobial strategies. Drugs 69:151–166. https://doi.org/10.2165/00003495-200969020-00002.
24. Mahmoud S, Hasabelnaby S, Hammad S, Sakr T. 2018. Antiviral nucleoside and nucleotide analogs: a review. J Adv Pharm Res 2:73–88. https://doi.org/10.21608/aprh.2018.5829.
25. Eltahla A, Luciani F, White P, Lloyd A, Bull R. 2015. Inhibitors of the hepatitis C virus polymerase; mode of action and resistance. Viruses 7:5206–5224. https://doi.org/10.3390/v7102868.
26. Smith EC, Blanc H, Surdel MC, Vignuzzi M, Denison MR. 2013. Coronaviruses lacking exoribonuclease activity are susceptible to lethal mutagenesis: evidence for proofreading and potential therapeutics. PLoS Pathog 9:e1003565. https://doi.org/10.1371/journal.ppat.1003565.
27. Warren TK, Wells J, Panchal RG, Stuthman KS, Garza NL, Van Tongeren SA, Dong L, Retterer CJ, Eaton BP, Pegoraro G, Honnold S, Bantia S, Kotian P, Chen X, Taubenheim BR, Welch LS, Minning DM, Babu YS, Sheridan WP, Bavari S. 2014. Protection against filovirus diseases by a novel broad-spectrum nucleoside analogue BCX4430. Nature 508:402–405. https://doi.org/10.1038/nature13027.
28. Warren TK, Jordan R, Lo MK, Ray AS, Mackman RL, Soloveva V, Siegel D, Perron M, Bannister R, Hui HC, Larson N, Strickley R, Wells J, Stuthman KS, Van Tongeren SA, Garza NL, Donnelly G, Shurtleff AC, Retterer CJ, Gharaibeh D, Zamani R, Kenny T, Eaton BP, Grimes E, Welch LS, Gomba L, Wilhelmsen CL, Nichols DK, Nuss JE, Nagle ER, Kugelman JR, Palacios G, Doerffler E, Neville S, Carra E, Clarke MO, Zhang L, Lew W, Ross B, Wang Q, Chun K, Wolfe L, Babusis D, Park Y, Stray KM, Trancheva I, Feng JY, Barauskas O, Xu Y, Wong P, Braun MR, Flint M, McMullan LK, Chen S-S, Fearns R, Swaminathan S, Mayers DL, Spiropoulou CF, Lee WA, Nichol ST, Cihlar T, Bavari S. 2016. Therapeutic efficacy of the small molecule GS-5734 against Ebola virus in rhesus monkeys. Nature 531:381–385. https://doi.org/10.1038/nature17180.
29. Sheahan TP, Sims AC, Graham RL, Menachery VD, Gralinski LE, Case JB, Leist SR, Pyrc K, Feng JY, Trantcheva I, Bannister R, Park Y, Babusis D, Clarke MO, Mackman RL, Spahn JE, Palmiotti CA, Siegel D, Ray AS, Cihlar T, Jordan R, Denison MR, Baric RS. 2017. Broad-spectrum antiviral GS-5734 inhibits both epidemic and zoonotic coronaviruses. Sci Transl Med 9:eaal3653. https://doi.org/10.1126/scitranslmed.aal3653.
30. Hofmann WP, Soriano V, Zeuzem S. 2009. Antiviral combination therapy for treatment of chronic hepatitis B, hepatitis C, and human immunodeficiency virus infection. Handb Exp Pharmacol 189:321–346. https://doi.org/10.1007/978-3-540-79086-0_12.
31. Urakova N, Kuznetsova V, Crossman DK, Sokratian A, Guthrie DB, Kolykhalov AA, Lockwood MA, Natchus MG, Crowley MR, Painter GR, Frolova EI, Frolov I. 2017. β-D-N(4)-Hydroxycytidine is a potent anti-alphavirus compound that induces high level of mutations in viral genome. J Virol 92:e01965-17. https://doi.org/10.1128/JVI.01965-17.
32. Ehteshami M, Tao S, Zandi K, Hsiao H-M, Jiang Y, Hammond E, Amblard F, Russell OO, Merits A, Schinazi RF. 2017. Characterization of β-D-N4-Hydroxycytidine as a novel inhibitor of chikungunya virus. Antimicrob Agents Chemother 61:e02395-16. https://doi.org/10.1128/AAC.02395-16.
33. Costantini VP, Whitaker T, Barclay L, Lee D, McBrayer TR, Schinazi RF, Vinjé J. 2012. Antiviral activity of nucleoside analogues against norovirus. Antivir Ther 17:981–991. https://doi.org/10.3851/IMP2229.
34. Yoon J-J, Toots M, Lee S, Lee M-E, Ludeke B, Luczo JM, Ganti K, Cox RM, Sticher ZM, Edpuganti V, Mitchell DG, Lockwood MA, Kolykhalov AA, Greninger AL, Moore ML, Painter GR, Lowen AC, Tompkins SM, Fearns R, Natchus MG, Plemper RK. 2018. Orally efficacious broad-spectrum ribonucleoside analog inhibitor of influenza and respiratory syncytial viruses. Antimicrob Agents Chemother 62:1427. https://doi.org/10.1128/AAC.00766-18.
35. Reynard O, Nguyen X-N, Alazard-Dany N, Barateau V, Cimarelli A, Volchkov VE. 2015. Identification of a new ribonucleoside inhibitor of Ebola virus replication. Viruses 7:6233–6240. https://doi.org/10.3390/v7122934.
36. Stuyver LJ, Whitaker T, McBrayer TR, Hernandez-Santiago BI, Lostia S, Tharnish PM, Ramesh M, Chu CK, Jordan R, Shi J, Rachakonda S, Watanabe KA, Otto MJ, Schinazi RF. 2003. Ribonucleoside analogue that blocks replication of bovine viral diarrhea and hepatitis C viruses in culture. Antimicrob Agents Chemother 47:244–254. https://doi.org/10.1128/aac.47.1.244-254.2003.
37. Agostini ML, Andres EL, Sims AC, Graham RL, Sheahan TP, Lu X, Smith EC, Case JB, Feng JY, Jordan R, Ray AS, Cihlar T, Siegel D, Mackman RL, Clarke MO, Baric RS, Denison MR. 2018. Coronavirus susceptibility to the antiviral remdesivir (GS-5734) is mediated by the viral polymerase and the proofreading exoribonuclease. mBio 9:1953. https://doi.org/10.1128/mBio.00221-18.
38. Graepel KW, Lu X, Case JB, Sexton NR, Smith EC, Denison MR. 2017. Proofreading-deficient coronaviruses adapt for increased fitness over long-term passage without reversion of exoribonuclease-inactivating mutations. mBio 8:e01503-17. https://doi.org/10.1128/mBio.01503-17.
39. Popowska E, Janion C. 1974. N4-hydroxycytidine—a new mutagen of a base analogue type. Biochem Biophys Res Commun 56:459–466. https://doi.org/10.1016/0006-291x(74)90864-x.
40. Daelemans D, Pauwels R, De Clercq E, Pannecouque C. 2011. A time-of-drug addition approach to target identification of antiviral compounds. Nat Protoc 6:925–933. https://doi.org/10.1038/nprot.2011.330.
41. Salganik RI, Vasjunina EA, Poslovina AS, Andreeva IS. 1973. Mutagenic action of N4-hydroxycytidine on Escherichia coli B cyt−. Mutat Res 20:1–5. https://doi.org/10.1016/0027-5107(73)90091-2.
42. Popowska E, Janion C. 1975. The metabolism of N4-hydroxycytidine—a mutagen for Salmonella typhimurium. Nucleic Acids Res 2:1143–1151. https://doi.org/10.1093/nar/2.7.1143.

43. Pyrc K, Bosch BJ, Berkhout B, Jebbink MF, Dijkman R, Rottier P, van der Hoek L. 2006. Inhibition of human coronavirus NL63 infection at early stages of the replication cycle. Antimicrob Agents Chemother 50:2000–2008. https://doi.org/10.1128/AAC.01598-05.
44. Barnard DL, Hubbard VD, Burton J, Smee DF, Morrey JD, Otto MJ, Sidwell RW. 2004. Inhibition of severe acute respiratory syndrome-associated coronavirus (SARSCoV) by calpain inhibitors and β-D-N4-hydroxycytidine. Antivir Chem Chemother 15:15–22. https://doi.org/10.1177/095632020401500102.
45. Sexton NR, Smith EC, Blanc H, Vignuzzi M, Peersen OB, Denison MR. 2016. Homology-based identification of a mutation in the coronavirus RNA-dependent RNA polymerase that confers resistance to multiple mutagens. J Virol 90:7415–7428. https://doi.org/10.1128/JVI.00080-16.
46. Ferron F, Subissi L, Silveira De Morais AT, Le NTT, Sevajol M, Gluais L, Decroly E, Vonrhein C, Bricogne G, Canard B, Imbert I. 2017. Structural and molecular basis of mismatch correction and ribavirin excision from coronavirus RNA. Proc Natl Acad Sci U S A 115:E162–E179. https://doi.org/10.1073/pnas.1718806115.
47. Derse D, Cheng Y-C, Furman PA, Clair MHS, Elion GB. 1981. Inhibition of purified human and herpes simplex virus-induced DNA polymerases by 9-(2-hydroxyethoxymethyl)guanine triphosphate. J Biol Chem 256:11447–11451.
48. Chamberlain JM, Sortino K, Sethna P, Bae A, Lanier R, Bambara RA, Dewhurst S. 2019. Cidofovir diphosphate inhibits adenovirus 5 DNA polymerase via both nonobligate chain termination and direct inhibition, and polymerase mutations confer cidofovir resistance on intact virus. Antimicrob Agents Chemother 63:331. https://doi.org/10.1128/AAC.01925-18.
49. Śledziewska-Gójska E, Janion C. 1982. Effect of proofreading and dam-instructed mismatch repair systems on N^4-hydroxycytidine-induced mutagenesis. Mol Gen Genet 186:411–418. https://doi.org/10.1007/BF00729462.
50. Bouvet M, Imbert I, Subissi L, Gluais L, Canard B, Decroly E. 2012. RNA 3′-end mismatch excision by the severe acute respiratory syndrome coronavirus nonstructural protein nsp10/nsp14 exoribonuclease complex. Proc Natl Acad Sci U S A 109:9372–9377. https://doi.org/10.1073/pnas.1201130109.
51. Tejero H, Montero F, Nuño JC. 2016. Theories of lethal mutagenesis: from error catastrophe to lethal defection. Curr Top Microbiol Immunol 392:161–179. https://doi.org/10.1007/82_2015_463.
52. Biktasova A, Hajek M, Sewell A, Gary C, Bellinger G, Deshpande HA, Bhatia A, Burtness B, Judson B, Mehra S, Yarbrough WG, Issaeva N. 2017. Demethylation therapy as a targeted treatment for human papillomavirus-associated head and neck cancer. Clin Cancer Res 23:7276–7287. https://doi.org/10.1158/1078-0432.CCR-17-1438.
53. Leyssen P, Balzarini J, De Clercq E, Neyts J. 2005. The predominant mechanism by which ribavirin exerts its antiviral activity in vitro against flaviviruses and paramyxoviruses is mediated by inhibition of IMP dehydrogenase. J Virol 79:1943–1947. https://doi.org/10.1128/JVI.79.3.1943-1947.2005.
54. Sanjuan R, Nebot MR, Chirico N, Mansky LM, Belshaw R. 2010. Viral mutation rates. J Virol 84:9733–9748. https://doi.org/10.1128/JVI.00694-10.
55. Hemida MG, Chu DKW, Poon LLM, Perera R, Alhammadi MA, Ng H-Y, Siu LY, Guan Y, Alnaeem A, Peiris M. 2014. MERS coronavirus in dromedary camel herd, Saudi Arabia. Emerg Infect Dis 20:1231–1234. https://doi.org/10.3201/eid2007.140571.
56. Cotten M, Watson SJ, Zumla AI, Makhdoom HQ, Palser AL, Ong SH, Al Rabeeah AA, Alhakeem RF, Assiri A, Al-Tawfiq JA, Albarrak A, Barry M, Shibl A, Alrabiah FA, Hajjar S, Balkhy HH, Flemban H, Rambaut A, Kellam P, Memish ZA. 2014. Spread, circulation, and evolution of the Middle East respiratory syndrome coronavirus. mBio 5:1814. https://doi.org/10.1128/mBio.01062-13.
57. Domingo E, Sheldon J, Perales C. 2012. Viral quasispecies evolution. Microbiol Mol Biol Rev 76:159–216. https://doi.org/10.1128/MMBR.05023-11.
58. Bloom JD, Lu Z, Chen D, Raval A, Venturelli OS, Arnold FH. 2007. Evolution favors protein mutational robustness in sufficiently large populations. BMC Biol 5:29–21. https://doi.org/10.1186/1741-7007-5-29.
59. Fares MA. 2015. The origins of mutational robustness. Trends Genet 31:373–381. https://doi.org/10.1016/j.tig.2015.04.008.
60. Schwarz B, Routledge E, Siddell SG. 1990. Murine coronavirus nonstructural protein ns2 is not essential for virus replication in transformed cells. J Virol 64:4784–4791.
61. Zhao L, Rose KM, Elliott R, Van Rooijen N, Weiss SR. 2011. Cell-type-specific type I interferon antagonism influences organ tropism of murine coronavirus. J Virol 85:10058–10068. https://doi.org/10.1128/JVI.05075-11.
62. Graham RL, Sims AC, Brockway SM, Baric RS, Denison MR. 2005. The nsp2 replicase proteins of murine hepatitis virus and severe acute respiratory syndrome coronavirus are dispensable for viral replication. J Virol 79:13399–13411. https://doi.org/10.1128/JVI.79.21.13399-13411.2005.
63. Manrubia SC, Domingo E, Lázaro E. 2010. Pathways to extinction: beyond the error threshold. Philos Trans R Soc B Biol Sci 365:1943–1952. https://doi.org/10.1098/rstb.2010.0076.
64. Sanjuán R, Moya A, Elena SF. 2004. The contribution of epistasis to the architecture of fitness in an RNA virus. Proc Natl Acad Sci U S A 101:15376–15379. https://doi.org/10.1073/pnas.0404125101.
65. Lyons D, Lauring A. 2018. Mutation and epistasis in influenza virus evolution. Viruses 10:E407. https://doi.org/10.3390/v10080407.
66. Chen W, Baric RS. 1996. Molecular anatomy of mouse hepatitis virus persistence: coevolution of increased host cell resistance and virus virulence. J Virol 70:3947–3960.
67. Yount B, Denison MR, Weiss SR, Baric RS. 2002. Systematic assembly of a full-length infectious cDNA of mouse hepatitis virus strain A59. J Virol 76:11065–11078. https://doi.org/10.1128/jvi.76.21.11065-11078.2002.
68. Almazán F, Márquez-Jurado S, Nogales A, Enjuanes L. 2015. Engineering infectious cDNAs of coronavirus as bacterial artificial chromosomes. Methods Mol Biol 1282:135–152. https://doi.org/10.1007/978-1-4939-2438-7_13.
69. Eckerle LD, Lu X, Sperry SM, Choi L, Denison MR. 2007. High fidelity of murine hepatitis virus replication is decreased in nsp14 exoribonuclease mutants. J Virol 81:12135–12144. https://doi.org/10.1128/JVI.01296-07.
70. Coleman CM, Frieman MB. 2015. Growth and quantification of MERS-CoV infection. Curr Protoc Microbiol 37:15E.2.1–9. https://doi.org/10.1002/9780471729259.mc15e02s37.
71. Bolger AM, Lohse M, Usadel B. 2014. Trimmomatic: a flexible trimmer for Illumina sequence data. Bioinformatics 30:2114–2120. https://doi.org/10.1093/bioinformatics/btu170.
72. Langmead B, Wilks C, Antonescu V, Charles R. 2019. Scaling read aligners to hundreds of threads on general-purpose processors. Bioinformatics 35:421–432. https://doi.org/10.1093/bioinformatics/bty648.
73. Wilm A, Aw PPK, Bertrand D, Yeo GHT, Ong SH, Wong CH, Khor CC, Petric R, Hibberd ML, Nagarajan N. 2012. LoFreq: a sequence-quality aware, ultra-sensitive variant caller for uncovering cell-population heterogeneity from high-throughput sequencing datasets. Nucleic Acids Res 40:11189–11201. https://doi.org/10.1093/nar/gks918.
74. Nakamura K, Oshima T, Morimoto T, Ikeda S, Yoshikawa H, Shiwa Y, Ishikawa S, Linak MC, Hirai A, Takahashi H, Altaf-Ul-Amin M, Ogasawara N, Kanaya S. 2011. Sequence-specific error profile of Illumina sequencers. Nucleic Acids Res 39:e90. https://doi.org/10.1093/nar/gkr344.